Effects of the trimodal random field on the magnetic properties of a spin-1 Ising nanotube*

H. Magoussi, A. Zaim†, and M. Kerouad‡

Laboratoire Physique des Matériaux et Modélisation des Systèmes (LP2MS), Unité Associée au CNRST-URAC: 08, *University Moulay Ismail, Faculty of Sciences, B.P.* 11201, *Zitoune, Meknes, Morocco*

(Received 28 February 2013; revised manuscript received 23 May 2013)

In this work, the hysteresis behavior of a nanotube, consisting of a ferromagnetic core of spin-1 atoms surrounded by a ferromagnetic shell of spin-1 atoms with ferro- or anti-ferromagnetic interfacial coupling is studied in the presence of a random magnetic field. Based on a probability distribution method, the effective-field theory has been used to investigate the effects of the random magnetic field, the interfacial coupling constant, and the temperature on the hysteresis loops of the nanotube. Some characteristic behaviors have been found, such as the existence of double or triple hysteresis loops for appropriate values of the system parameters. The remanent magnetization and the coercive field, as functions of the temperature, are examined.

Keywords: effective-field theory, nanotube, critical phenomena

PACS: 64.60.De, 61.46.Fg, 68.35.Rh **DOI:** 10.1088/1674-1056/22/11/116401

1. Introduction

Magnetic nanomaterials have recently attracted considerable attention and intensive research due to their promising applications in diverse areas of high-density magnetic storage media,[1,2] magnetic resonance imaging,[3] nonlinear optics,[4] ferrofluids,[5] environmental remediation,[6] catalysis,[7] and biomedicine.[8] Theoretically, the magnetic properties of nanoparticles have been widely investigated by the use of various techniques, including the mean-field theory,[9] effective-field theory,[10–12] Monte Carlo simulations,[13–17] Green's function technique,[18,19] and Bethe–Perils approximation.[20] For example, Zaim *et al.*[16] have discussed the magnetic behavior of a ferrimagnetic core/shell nanoparticle. They have found that the system can exhibit one or even two compensation temperatures. Canko *et al.*,[11] have investigated the Blume–Capel model on a cylindrical Ising nanotube. They have obtained that the tricritical point depends on the coupling constant between the core and the surface shell. In a recent work, Kaneyoshi[10] observed that the existence of reentrant behavior and compensation point in a decorated Ising nanowire is dependent on the system parameters.

The hysteresis behaviors in magnetic nanoparticles is a common interest of many research works.[21–27] Recently, Keskin *et al.*[23] have investigated the hysteresis loops of the cylindrical Ising nanowire defined by Kaneyoshi,[28,29] for the reduced temperatures below, around, and above the critical temperature. They have observed that the results of hysteresis behaviors of nanowires are in good agreement with both theoretical and experimental results. Within the mean field approximation, Usov *et al.*[30] have studied the magnetic properties of a composite nanoparticle having an inner ferromagnetic core and an outer antiferromagnetic shell. It is shown that the coercive force increases as a function of the antiferromagnetic shell thickness. Moreover, The dependence of remanence and coercivity on the exchange and dipolar magnetic fields of the nanoparticle systems is studied in Ref. [31]. It is found that both remanence and coercivity decrease with the increase of temperature. Based on the Monte Carlo simulation, the effects of size and surface anisotropy on hysteresis loops of a small spherical particle have been investigated.[32] These simulations showed that the hysteresis loops and coercivity are strongly affected by the particle size and the thickness of the surface layer with large anisotropy. Using the effective-field theory with correlations and the Glauber-type stochastic approach,[33,34] Deviren *et al.* have studied hysteresis loop areas and correlations of a cylindrical Ising nanotube or nanowire in an oscillating magnetic field.

During the last few years, the interest in magnetic systems at a nanometric scale has grown due to their interesting magnetic properties, which are significantly different from those of the bulk. In recent works, the effective-field theory with correlations has been used to study the magnetic properties of the mixed spin (1, 3/2) ferrimagnetic cubic nanowire[35] and the mixed spin (3/2, 5/2) ferrimagnetic nanoparticle.[36] One or two compensation points have been found for certain values of the system parameters. In Ref. [37], the influences of the crystal fields on the phase diagram of a mixed

*Project supported by URAC: 08, the project RS: 02 (CNRST), and the Swedish Research Links programme dnr-348-2011-7264.

†Corresponding author. E-mail: ah_zaim@yahoo.fr

‡Corresponding author. E-mail: kerouad@fs-umi.ac.ma

© 2013 Chinese Physical Society and IOP Publishing Ltd

spin (1, 3/2) ferrimagnetic nanoparticle have been investigated by using Monte Carlo simulation. It has been found that the system exhibits tricritical and compensation points. Jiang *et al.*[38] have studied the effect of the single-ion anisotropies on the magnetization plateaus of a ferrimagnetic mixed-spin nanoparticle at very low temperature in detail. In Ref. [39] Guo *et al.* developed a method to study the magnetic susceptibility and the hysteresis loop of mixed ferri-ferrimagnets composed of Prussian blue analogs with an orthorhombic structure. The results have shown that the magnetic susceptibility including the initial magnetic susceptibility of the novel magnet $S^{III}_{m_y}Gd^{III}_{1-y}[Cr^{III}(CN)_6]$.

In particular, we pay attention to the work of Kaneyoshi,[29] where the magnetization and susceptibility of a cylindrical core/shell spin-1/2 Ising nanotube within the effective-field theory with correlations have been investigated. However, the study of the effects of the random magnetic field on the hysteresis behaviors of a spin-1 Ising nanotube with core/shell morphology has not been done. Therefore, the purpose of this paper is to investigate the hysteresis behaviors of an Ising nanotube, using an effective-field theory based on a probability distribution method. We also investigate the temperature dependence of the coercivity and remanent magnetization.

The rest of the paper is arranged as follows. In Section 2, we give the model and the formalism. In Section 3, we present the results and discussion, while Section 4 is devoted to a brief conclusion.

2. Model and formalism

We consider an Ising nanotube model in a random magnetic field consisting of a spin-1 ferromagnetic core which is surrounded by a spin-1 ferromagnetic surface shell (Fig. 1). Each spin is connected to the two nearest-neighbor spins on the above and below sections. The Hamiltonian of the model is given by

$$H = -J_c\sum_{\langle i,j\rangle}S_iS_j - J_s\sum_{\langle m,n\rangle}S_mS_n - J_{int}\sum_{\langle i,m\rangle}S_iS_m - \sum_i h_iS_i - \sum_m h_mS_m - H\left(\sum_i S_i + \sum_m S_m\right), \quad (1)$$

where the J_c and J_s are the exchange interaction parameters between two nearest neighbor magnetic atoms at the core and the surface shell, and J_{int} is the exchange interaction between two neighbor magnetic atoms at the surface shell and the core, S_i is the spin, which takes the values $\pm1,0$ at each site i of the Ising nanoparticle model and a summation indexes $\langle i,j\rangle$, $\langle m,n\rangle$, and $\langle i,m\rangle$ denote a summation over all pairs of neighboring spins at the core, shell surface, and between the shell and the core, respectively, H is an external magnetic field, h_i and h_m are the random longitudinal magnetic fields acting on S_i and S_m respectively distributed according to a trimodal distribution

$$P(h_i) = p\delta(h_i) + \frac{1}{2}(1-p)(\delta(h_i-h_0)+\delta(h_i+h_0)), \quad (2)$$

$$P(h_m) = p\delta(h_m) + \frac{1}{2}(1-p)(\delta(h_m-h_0)+\delta(h_m+h_0)). \quad (3)$$

Two longitudinal magnetizations on the shell surface, namely m_{s_1} and m_{s_2} and a longitudinal magnetization on the core, namely m_c within the framework of the effective-field theory with a probability distribution, can be obtained as

$$\begin{aligned} m_{s_1} = {} & 2^{-5}\sum_{\mu_1=0}^{2}\sum_{\mu_2=0}^{2}\sum_{\mu_3=0}^{1}\sum_{\nu_1=0}^{2-\mu_1}\sum_{\nu_2=0}^{2-\mu_2}\sum_{\nu_3=0}^{1-\mu_3}2^{(\mu_1+\mu_2+\mu_3)} \\ & \times C^2_{\mu_1}C^2_{\mu_2}C^1_{\mu_3}C^{2-\mu_1}_{\nu_1}C^{2-\mu_2}_{\nu_2}C^{1-\mu_3}_{\nu_3}(1-q_{s_1})^{\mu_1} \\ & \times (1-q_{s_2})^{\mu_2}(1-q_c)^{\mu_3}(q_{s_1}-m_{s_1})^{\nu_1}(q_{s_2}-m_{s_2})^{\nu_2} \\ & \times (q_c-m_c)^{\nu_3}(q_{s_1}+m_{s_1})^{2-\mu_1-\nu_1} \\ & \times (q_{s_2}+m_{s_2})^{2-\mu_2-\nu_2}(q_c+m_c)^{1-\mu_3-\nu_3} \\ & \times F_m(x_1,h,h_0), \end{aligned} \quad (4)$$

$$\begin{aligned} m_{s_2} = {} & 2^{-6}\sum_{\mu_1=0}^{2}\sum_{\mu_2=0}^{2}\sum_{\mu_3=0}^{2}\sum_{\nu_1=0}^{2-\mu_1}\sum_{\nu_2=0}^{2-\mu_2}\sum_{\nu_3=0}^{2-\mu_3}2^{(\mu_1+\mu_2+\mu_3)}C^2_{\mu_1}C^2_{\mu_2}C^2_{\mu_3} \\ & \times C^{2-\mu_1}_{\nu_1}C^{2-\mu_2}_{\nu_2}C^{2-\mu_3}_{\nu_3}(1-q_{s_1})^{\mu_1} \\ & \times (1-q_{s_2})^{\mu_2}(1-q_c)^{\mu_3}(q_{s_1}-m_{s_1})^{\nu_1}(q_{s_2}-m_{s_2})^{\nu_2} \\ & \times (q_c-m_c)^{\nu_3}(q_{s_1}+m_{s_1})^{2-\mu_1-\nu_1} \\ & \times (q_{s_2}+m_{s_2})^{2-\mu_2-\nu_2}(q_c+m_c)^{2-\mu_3-\nu_3} \\ & \times F_m(x_2,h,h_0), \end{aligned} \quad (5)$$

$$\begin{aligned} m_c = {} & 2^{-7}\sum_{\mu_1=0}^{1}\sum_{\mu_2=0}^{2}\sum_{\mu_3=0}^{4}\sum_{\nu_1=0}^{1-\mu_1}\sum_{\nu_2=0}^{2-\mu_2}\sum_{\nu_3=0}^{4-\mu_3}2^{(\mu_1+\mu_2+\mu_3)}C^1_{\mu_1}C^2_{\mu_2}C^4_{\mu_3} \\ & \times C^{1-\mu_1}_{\nu_1}C^{2-\mu_2}_{\nu_2}C^{4-\mu_3}_{\nu_3}(1-q_{s_1})^{\mu_1} \\ & \times (1-q_{s_2})^{\mu_2}(1-q_c)^{\mu_3}(q_{s_1}-m_{s_1})^{\nu_1}(q_{s_2}-m_{s_2})^{\nu_2} \\ & \times (q_c-m_c)^{\nu_3}(q_{s_1}+m_{s_1})^{1-\mu_1-\nu_1} \\ & \times (q_{s_2}+m_{s_2})^{2-\mu_2-\nu_2}(q_c+m_c)^{4-\mu_3-\nu_3} \\ & \times F_m(x_3,h,h_0). \end{aligned} \quad (6)$$

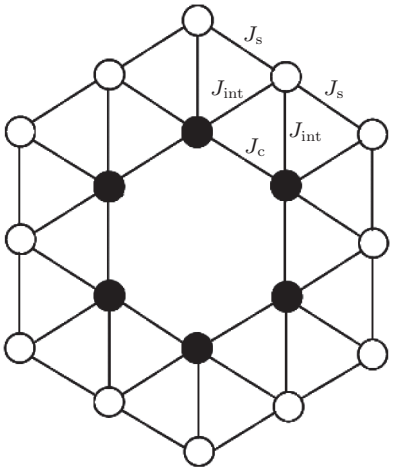


Fig. 1. Schematic representation of a cross-section of a nanotube. Open circles indicate magnetic atoms at the surface shell and solid circles are magnetic atoms constituting the core.

Two longitudinal quadrupolar moments on the shell surface, namely q_{s_1} and q_{s_2} and a quadrupolar moment on the core, namely q_c, can be obtained as

$$\begin{aligned} q_{s_1} &= 2^{-5}\sum_{\mu_1=0}^{2}\sum_{\mu_2=0}^{2}\sum_{\mu_3=0}^{1}\sum_{\nu_1=0}^{2-\mu_1}\sum_{\nu_2=0}^{2-\mu_2}\sum_{\nu_3=0}^{1-\mu_3} 2^{(\mu_1+\mu_2+\mu_3)}C_{\mu_1}^{2}C_{\mu_2}^{2}C_{\mu_3}^{1} \\ &\times C_{\nu_1}^{2-\mu_1}C_{\nu_2}^{2-\mu_2}C_{\nu_3}^{1-\mu_3}(1-q_{s_1})^{\mu_1}(1-q_{s_2})^{\mu_2} \\ &\times (1-q_c)^{\mu_3}(q_{s_1}-m_{s_1})^{\nu_1}(q_{s_2}-m_{s_2})^{\nu_2} \\ &\times (q_c-m_c)^{\nu_3}(q_{s_1}+m_{s_1})^{2-\mu_1-\nu_1} \\ &\times (q_{s_2}+m_{s_2})^{2-\mu_2-\nu_2}(q_c+m_c)^{1-\mu_3-\nu_3} \\ &\times F_q(x_1,h,h_0), \end{aligned} \tag{7}$$

$$\begin{aligned} q_{s_2} &= 2^{-6}\sum_{\mu_1=0}^{2}\sum_{\mu_2=0}^{2}\sum_{\mu_3=0}^{2}\sum_{\nu_1=0}^{2-\mu_1}\sum_{\nu_2=0}^{2-\mu_2}\sum_{\nu_3=0}^{2-\mu_3} 2^{(\mu_1+\mu_2+\mu_3)}C_{\mu_1}^{2}C_{\mu_2}^{2}C_{\mu_3}^{2} \\ &\times C_{\nu_1}^{2-\mu_1}C_{\nu_2}^{2-\mu_2}C_{\nu_3}^{2-\mu_3}(1-q_{s_1})^{\mu_1} \\ &\times (1-q_{s_2})^{\mu_2}(1-q_c)^{\mu_3}(q_{s_1}-m_{s_1})^{\nu_1}(q_{s_2}-m_{s_2})^{\nu_2} \\ &\times (q_c-m_c)^{\nu_3}(q_{s_1}+m_{s_1})^{2-\mu_1-\nu_1} \\ &\times (q_{s_2}+m_{s_2})^{2-\mu_2-\nu_2}(q_c+m_c)^{2-\mu_3-\nu_3} \\ &\times F_q(x_2,h,h_0), \end{aligned} \tag{8}$$

$$\begin{aligned} q_c &= 2^{-7}\sum_{\mu_1=0}^{1}\sum_{\mu_2=0}^{2}\sum_{\mu_3=0}^{4}\sum_{\nu_1=0}^{1-\mu_1}\sum_{\nu_2=0}^{2-\mu_2}\sum_{\nu_3=0}^{4-\mu_3} 2^{(\mu_1+\mu_2+\mu_3)}C_{\mu_1}^{1}C_{\mu_2}^{2}C_{\mu_3}^{4} \\ &\times C_{\nu_1}^{1-\mu_1}C_{\nu_2}^{2-\mu_2}C_{\nu_3}^{4-\mu_3}(1-q_{s_1})^{\mu_1} \\ &\times (1-q_{s_2})^{\mu_2}(1-q_c)^{\mu_3}(q_{s_1}-m_{s_1})^{\nu_1}(q_{s_2}-m_{s_2})^{\nu_2} \\ &\times (q_c-m_c)^{\nu_3}(q_{s_1}+m_{s_1})^{1-\mu_1-\nu_1} \\ &\times (q_{s_2}+m_{s_2})^{2-\mu_2-\nu_2}(q_c+m_c)^{4-\mu_3-\nu_3} \\ &\times F_q(x_3,h,h_0), \end{aligned} \tag{9}$$

where

$$\begin{aligned} x_1 &= J_s(2-\mu_1-2\nu_1)+J_s(2-\mu_2-2\nu_2) \\ &\quad +J_{int}(1-\mu_3-2\nu_3), \\ x_2 &= J_s(2-\mu_1-2\nu_1)+J_s(2-\mu_2-2\nu_2) \\ &\quad +J_{int}(2-\mu_3-2\nu_3), \\ x_3 &= J_{int}(1-\mu_1-2\nu_1)+J_{int}(2-\mu_2-2\nu_2) \\ &\quad +J_c(4-\mu_3-2\nu_3), \end{aligned}$$

$$\begin{aligned} F_m(x_j,h,h_0) &= pf_m(x_j,h,0)+\frac{1}{2}(1-p)(f_m(x_j,h,-h_0) \\ &\quad +f_m(x_j,h,h_0)), \end{aligned} \tag{10}$$

$$\begin{aligned} F_q(x_j,h,h_0) &= pf_q(x_j,h,0)+\frac{1}{2}(1-p)(f_q(x_j,h,-h_0) \\ &\quad +f_q(\beta x_j,h,h_0)), \quad j=1,2,3. \end{aligned} \tag{11}$$

The functions f_m and f_q are given by

$$f_m(x_j,h,h_0)=\frac{2\sinh(\beta x_j+H+h_0)}{1+2\cosh(\beta x_j+H+h_0)}, \tag{12}$$

$$f_q(x_j,h,h_0)=\frac{2\cosh(\beta x_j+H+h_0)}{1+2\cosh(\beta x_j+H+h_0)}, \tag{13}$$

with $\beta=1/(k_BT)$, T is the absolute temperature and k_B is the Boltzmann factor, C_k^l denotes the binomial coefficient, $C_k^l=l!/(k!(l-k)!)$.

Furthermore, let us define the longitudinal magnetization per site of the shell surface M_{sh}, and the total magnetization per site M_t as follows:

$$M_{sh}=\frac{1}{2}(m_{s_1}+m_{s_2}), \tag{14}$$

$$M_t=\frac{1}{3}(m_{s_1}+m_{s_2}+m_c). \tag{15}$$

According to the third law of thermodynamics, the Gibbs free energy can be written in the form[40]

$$F=U-T\int_0^T\frac{C_v(t)}{t}\,dt, \tag{16}$$

where U is the internal energy per site and

$$C_v(T)=\frac{\partial U}{\partial T}$$

is the specific heat per site of the system. The internal energy per site within the framework of the EFT is

$$\begin{aligned} U &=\langle H_i\rangle=\langle ES\rangle-\frac{h_0}{3}(m_{s_1}+m_{s_2}+m_c) \\ &=-\frac{1}{6}(u_{s_1}+u_{s_2}+u_c)-\frac{h_0}{3}(m_{s_1}+m_{s_2}+m_c). \end{aligned}$$

It is easy to obtain the expression of u_{s_1}, u_{s_2}, and u_c by subsisting the function $F(x_i,h_0)$ with $W(x_i)=x_iF(x_i,h_0)$ in the expressions of the longitudinal magnetizations m_{s_1}, m_{s_2}, and m_c.

3. Results and discussion

Our investigations in this work are for both ferromagnetic and ferrimagnetic cases. Hence, $J_{int}>0$ and $J_{int}<0$ correspond to the ferromagnetic and antiferromagnetic interfacial couplings, respectively.

3.1. Ferromagnetic case

In this section, we investigate the influence of the random magnetic field on the phase transition and the hysteresis loops of a ferromagnetic nanotube. In the following, in the absence of the external magnetic field ($H=0$), we show in Fig. 2(a), the total magnetization per spin M_t as a function of the temperature T/J_c for two values of the random magnetic field ($h_0/J_c=3.2$ and 3.8), and the fixed parameters, $J_s/J_c=J_{int}/J_c=1$ and $p=0.25$. For $h_0/J_c=3.2$, it is observed that when we increase the temperature, the total magnetization decreases continuously and vanishes at a second-order ferromagnetic–paramagnetic phase transition ($T_c/J_c=2.28$). It is seen that when $h_0/J_c=3.8$, the total magnetization undertakes a jump, at a first-order temperature $T_c/J_c=0.69$, between the ferromagnetic ($M_T\neq 0$) and the paramagnetic ($M_T=0$) phases of the magnetic nanotube. In Fig. 2(b), we

plot the internal energy U per spin as a function of the temperature T/J_c for the same parameters of Fig. 2(a). It is remarked that the curves of the internal energy present a discontinuous behavior, which is clearly observed at the first-order transition ($T_c/J_c = 0.69$). Figure 2(c) presents the phase diagram in the $(T_c/J_c, h_0/J_c)$ plane with fixed parameters $J_s/J_c = J_{int}/J_c = 1$ and $p = 0.25$. We can see that the critical temperature decreases progressively with h_0/J_c increasing, starting from a high saturation value at $h_0/J_c = 0$ to reach zero at $h_0/J_c = 4$. It is also seen that we have a tricritical point (TCP) (heavy black), which joins the second-order phase transition branch (solid line) with the first-order phase transition branch (dashed line) of the phase diagram. We should mention that a similar phase diagram was obtained in Ref. [41].

In order to examine the effect of the temperature T/J_c on the hysteresis behavior of the ferromagnetic nanotube, a series of hysteresis loops are plotted in Fig. 3(a) with fixed parameters, $J_s/J_c = J_{int}/J_c = 1$, $h_0/J_c = 3.2$, and $p = 0.25$. From this figure, we can see that the magnetization curves are symmetric for both positive and negative values of the external magnetic field. We can also see that the hysteresis loops disappear for a temperature above the transition temperature $T_c/J_c = 2.28$ and that the shape of the hysteresis loop becomes narrower as the temperature increases below the transition one. In Fig. 3(b), we display the temperature dependence of the coercive magnetic field H_c and the remanent magnetization M_R for fixed parameters values, $J_s/J_c = J_{int}/J_c = 1$, $h_0/J_c = 3.2$ and $p = 0.25$. The coercive magnetic field is defined as the field at which the sign of the magnetization changes. It is clear that the coercive field decreases with the temperature increasing and vanishes at $T_c/J_c = 2.28$. Our results are in agreement with those obtained in Ref. [42]. It is also clear that the remanent magnetization decreases with the increase of the temperature from its saturation value at low temperature region, and vanishes for $T/J_c \geq T_c/J_c$.

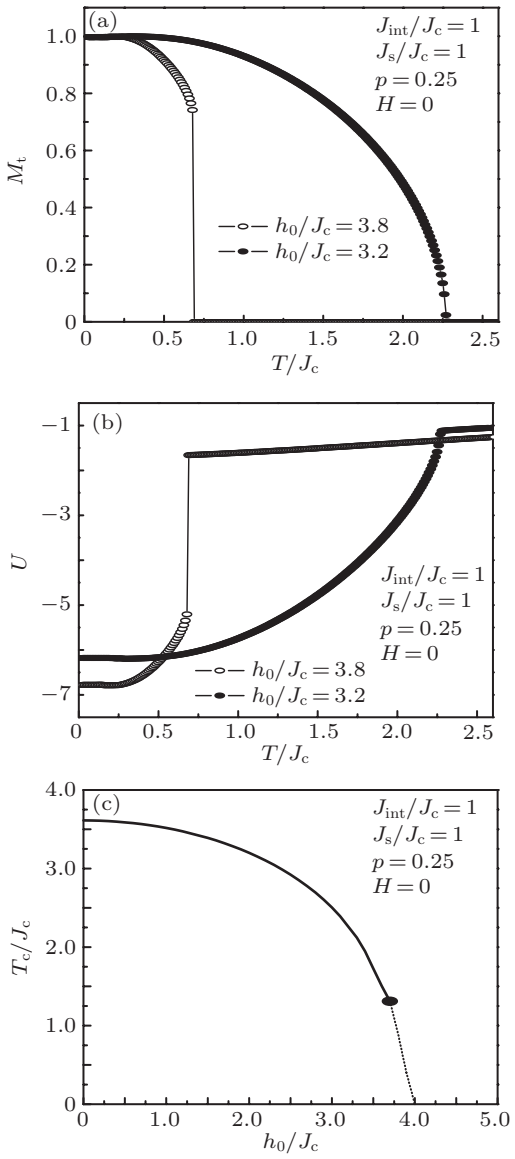


Fig. 2. (a) The total magnetization M_t as a function of the temperature T/J_c for two values of h_0/J_c (3.2 and 3.8), and the fixed parameters, $J_s/J_c = J_{int}/J_c = 1$ and $p = 0.25$. (b) The internal energy per site of the system as a function of the temperature T/J_c for two values of h_0/J_c (3.2 and 3.8), and the fixed parameters, $J_s/J_c = J_{int}/J_c = 1$ and $p = 0.25$. (c) The phase diagram in the (T_c–h_0) plane of the system for $J_s/J_c = J_{int}/J_c = 1$, the solid and dashed lines correspond to the second- and first-order phase transitions, respectively. The tricritical point is marked by heavy black.

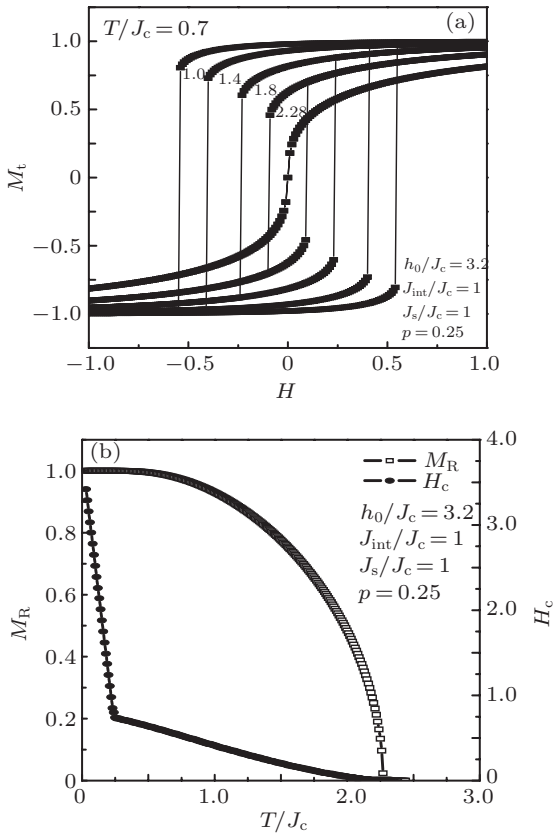


Fig. 3. (a) Hysteresis loops of the nanotube for $h_0/J_c = 3.2$, $J_s/J_c = J_{int}/J_c = 1$, $p = 0.25$, and for different values of the temperature T. (b) The dependence of the coercive field H_c and the remanent magnetization M_R on the temperature T/J_c for $h_0/J_c = 3.2$, $p = 0.25$, and $J_s/J_c = J_{int}/J_c = 1$.

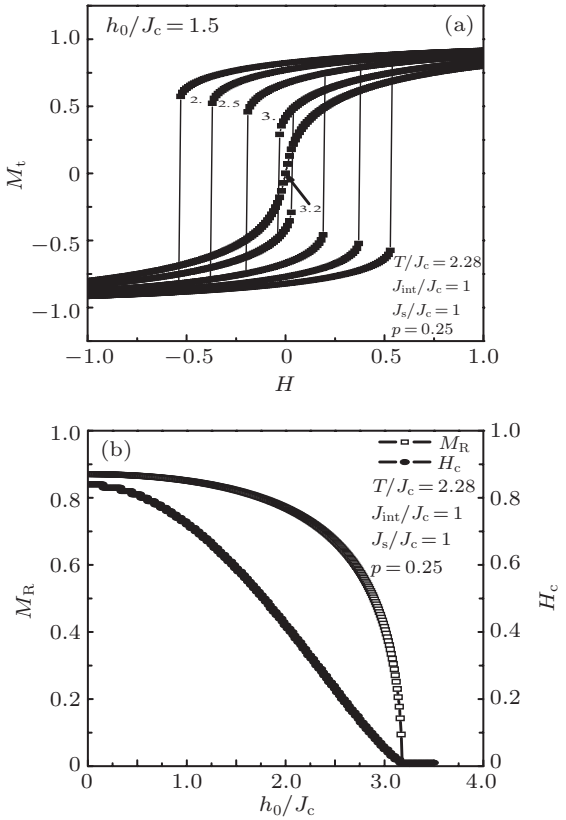


Fig. 4. (a) Hysteresis loops of the nanotube for $T/J_c = 2.28$, $J_s/J_c = J_{int}/J_c = 1$, $p = 0.25$, and for different values of the random magnetic field h_0/J_c. (b) The dependence of the coercive field H_c and the remanent magnetization M_R on the the random magnetic field h_0/J_c for $T/J_c = 2.28$, $p = 0.25$, and $J_s/J_c = J_{int}/J_c = 1$.

The dependence of the hysteresis loops on the random magnetic field h_0/J_c for $J_s/J_c = J_{int}/J_c = 1$, $T/J_c = 2.28$, and for $p = 0.25$ is shown in Fig. 4(a), it is apparent that with the increase of the random magnetic field, the hysteresis loop is more compact and narrow. The coercive field decreases with the increase of the applied random field and vanishes at the critical field value $h_0^c = 3.2$ (Fig. 4(b)). For $h_0/J_c \geq h_0^c/J_c$, the hysteresis loop disappears. We can also notice that when the random magnetic field increases, the remanent magnetization decreases from its saturation value at the low random magnetic field region, and vanishes at the critical random magnetic field.

To show the presence of the double hysteresis curves in this system, we have investigated the hysteresis curves at different values of the temperature below, around, and above the critical temperature, for h_0/J_c =3.8, J_{int}/J_c = J_s/J_c=1, and $p = 0.25$. From Fig. 5(a), at a temperature below the critical one T/J_c = 0.3, it is seen that we have only one ferromagnetic hysteresis loop. It is clear also that two steps appear when the temperature approaches its critical value $T_c/J_c = 0.69$ (Fig. 5(b)). For $T/J_c \geq T_c/J_c$ (Figs. 5(c)–5(d)), it is observed that the shape of the hysteresis loops changes from ferromagnetic hysteresis loop to double hysteresis loops and that when the temperature increases from 0.69 to 1, the hysteresis loops disappear. The double hysteresis loops have been seen experimentally in different systems, for example in Mn-doped (pb, La) $(Zr,Ti)O_3$ ceramics,[43] and in Fe_3O_4/Mn_3O_3 superlattices.[44]

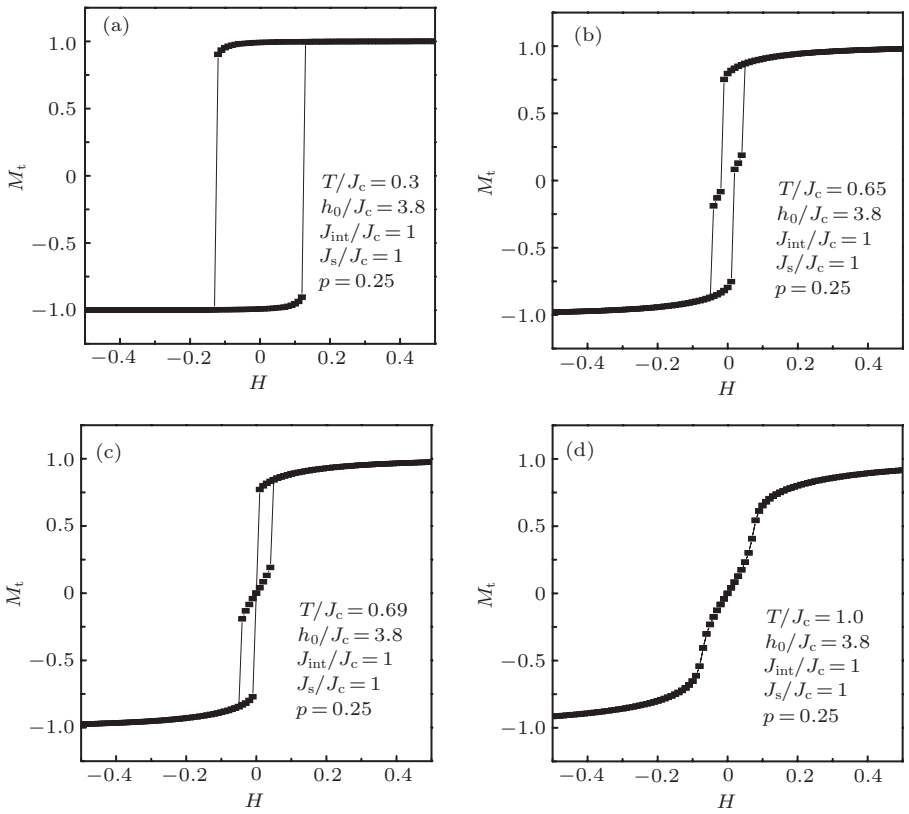


Fig. 5. The magnetic hysteresis curves of the ferromagnetic nanotube for $h_0/J_c = 3.8$, $J_s/J_c = 1$, and $p = 0.25$, and for different values of the temperature T/J: (a) $T/J = 0.3$, (b) $T/J = 0.65$, (c) $T/J = 0.69$, and (d) $T/J = 1$.

3.2. Ferrimagnetic case

In this section, we investigate the effects of the interfacial coupling, the random magnetic field, and the shell coupling on the hysteresis loops of a ferrimagnetic nanotube with core/shell morphology. In Fig. 6, we show the dependence of the hysteresis loops of a ferrimagnetic nanotube on the antiferromagnetic interfacial coupling constant $J_{\rm int}/J_{\rm c}$ at $T/J_{\rm c} = 1.8$ for $J_{\rm s}/J_{\rm c} = 1$, $h_0/J_{\rm c} = 0$, and $p = 0.25$. We can see that if the antiferromagnetic coupling constant is small (Fig. 6(a)), a central loop opens only. The central loop involves two steps due to the different ferromagnetic properties of the core and the shell. This phenomenon illustrates that the behavior of the nanotube approaches that of ferromagnetic behavior as the absolute value of the antiferromagnetic interfacial coupling constant decreases. It is shown that when $|J_{\rm int}|/J_{\rm c}$ increases (Figs. 6(b) and 6(c)) the hysteresis curve changes from one central loop to triple loops. The larger the antiferromagnetic coupling constant is, the more difficult for the applied magnetic field to change the direction of the magnetization at the interfacial layers in the core and the shell is. So the outer loops stretch further out horizontally with increasing $|J_{\rm int}|/J_{\rm c}$. It implied that the behavior of the system is ferromagnetic like for smaller $|J_{\rm int}|/J_{\rm c}$, and antiferromagnetic like for larger $|J_{\rm int}|/J_{\rm c}$. The results mentioned above are qualitatively in good agreement with hysteresis loops of ferroelectric or ferrielectric core/shell nanotubes.[45]

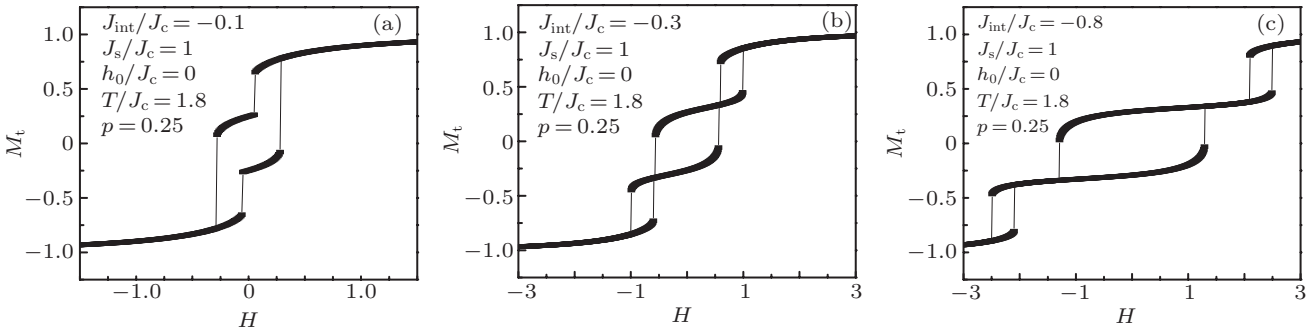


Fig. 6. The magnetic hysteresis curves of the ferrimagnetic nanotube for the fixed parameters $h_0/J_{\rm c}$=0, $J_{\rm s}/J_{\rm c}$= 1, $T/J_{\rm c} = 1.8$ and $p = 0.25$, and for different values of the antiferromagnetic interfacial coupling constant: (a) $J_{\rm int}/J_{\rm c} = -0.1$, (b) $J_{\rm int}/J_{\rm c} = -0.3$, and (c) $J_{\rm int}/J_{\rm c} = -0.8$.

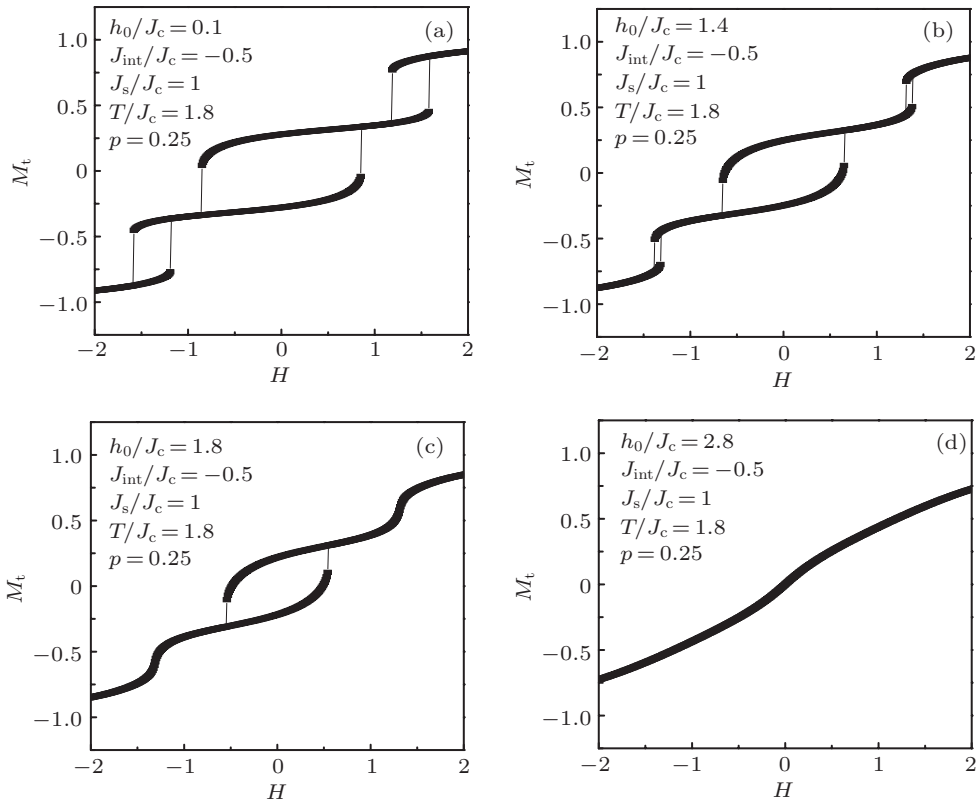


Fig. 7. The magnetic hysteresis curves of the ferrimagnetic nanotube for the fixed parameters $J_{\rm int}/J_{\rm c} = -0.5$, $J_{\rm s}/J_{\rm c}$= 1, $T/J_{\rm c} = 1.8$, and $p = 0.25$, and for different values of the random magnetic field: (a) $h_0/J_{\rm c} = 0.1$, (b) $h_0/J_{\rm c} = 1.4$, (c) $h_0/J_{\rm c} = 1.8$, and (d) $h_0/J_{\rm c} = 2.8$.

To better understand the effect of the random magnetic field on the hysteresis loops, we plot in Fig. 7, the magnetization curves versus the applied magnetic field H for $J_s/J_c = 1$, $J_{int}/J_c = -0.5$, $T/J_c = 1.8$ and for different values of the random magnetic field ($h_0/J_c = 0.1$, 1.4, 1.8, and 2.8). From Fig. 7, we can see that the size of the outer loops and that of the central loop is narrower when the random magnetic field varies from 0.1 to 1.4. As shown in Fig. 7(c), for $h_0/J_c = 1.8$, the outer loops disappear and the central one reduces. When $h_0/J_c = 2.8$ in Fig. 7(d), the hysteresis loops disappear.

In order to investigate the effect of the exchange interaction J_s/J_c at the surface, we plot in Fig. 8, the magnetization curves versus the applied magnetic field H for $h_0/J_c = 0.5$, $J_{int}/J_c = -0.3$, $T/J_c = 1.8$ and for different values of the shell coupling ($J_s/J_c = 0.85$, 1.2, and 1.8). It is observed that the shapes of the hysteresis loops change from triple hysteresis loops to one central loop and that when J_s/J_c increases, the area of the central loop increases. Moreover the triple hysteresis loop behavior has been seen for different systems, such as in single chain magnets with antiferomagnetic interchain coupling[46] and in molecular-based magnetic materials.[47] In addition, triple hysteresis loop behaviors have been also seen experimentally in CoFeB/Cu, CoNip/Cu, FeGa/py, and FeGa/CoFeB multilayered nanowires.[48]

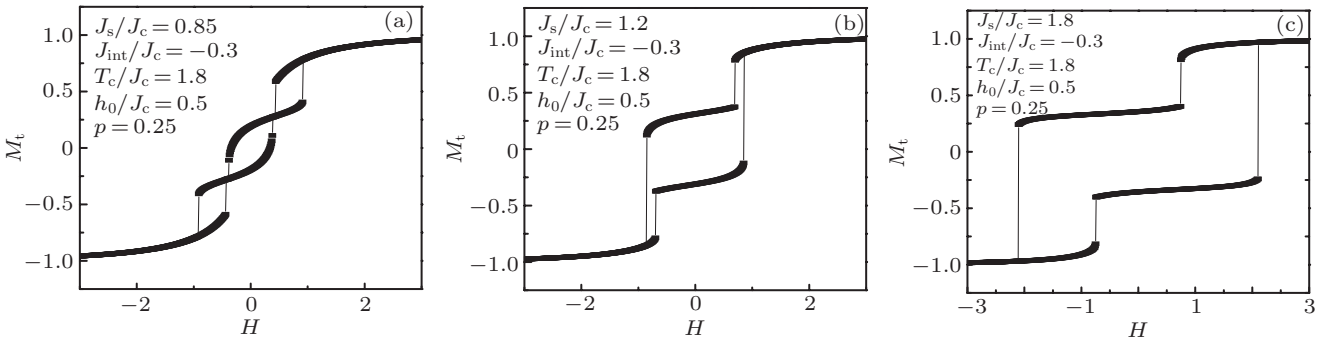


Fig. 8. The magnetic hysteresis curves of the ferrimagnetic nanotube for the fixed parameters $J_{int}/J_c = -0.3$, $h_0/J_c = 0.5$, $T/J_c = 1.8$ and $p = 0.25$, and for different values of the shell coupling: (a) $J_s/J_c = 0.85$, (b) $J_s/J_c = 1.2$, and (c) $J_s/J_c = 1.8$.

4. Conclusion

In summary, we have studied the hysteresis behavior of spin-1 Ising nanotubes with core/shell morphology in a random magnetic field where we have taken coupling constants J_c and J_s for the core and the shell respectively, and an interfacial coupling constant J_{int} between the nearest-neighbors spin across the core-shell. Using an effective-field theory based on a probability distribution method, we discussed both ferromagnetic and ferrimagnetic cases, the influence of the random magnetic field, the temperature, and the interfacial coupling constant on the hysteresis behaviors. It is shown that for the ferromagnetic case, the shapes of the hysteresis loops change from a ferromagnetic hysteresis loop to double hysteresis loops and that when T increases, the double hysteresis loops disappear. It is also shown that, the coercive field decreases with the temperature increasing. For the ferrimagnetic case, it is clear that the triple hysteresis loop behavior occurs for the larger antiferromagnetic coupling constant and that when the surface coupling J_s is increased, the behavior changes from triple to simple hysteresis loops.

References

[1] Kodama R H, Berkowitz A E, McNiff E J and Foner J S 1996 *Phys. Rev. Lett.* **77** 394
[2] Hayashi T, Hirono S, Tomita M and Umemura S 1996 *Nature* **381** 772
[3] Kim J, Park S, Lee J E, Jin S M, Lee J H, Lee I S, Yang I, Kim J S, Kim S K, Cho M H and Hyeon T 2006 *Angew. Chem. Int. Ed.* **45** 7754
[4] Nie S and Emory S R 1997 *Science* **275** 1102
[5] Rosensweig R E 1997 *Ferrohydrodynamics* (New York: Dover)
[6] Elliott D W and Zhang W X 2001 *Environ. Sci. Technol.* **35** 4922
[7] Lu A H, Schmidt W, Matoussevitch N, Bönnemann H, Spliethoff B, Tesche B, Bill E, Kiefer W and Schüth F 2004 *Nanoengineering of a Magnetically Separable Hydrogenation Catalyst* (Angewandte Chemie International Edition in English) **43** 4303
[8] Wong A P Y and Chan M H W 1990 *Phys. Rev. Lett.* **65** 2567
[9] Michael F, Gonzalez C, Mujica V, Marquez M and Ratner M A 2007 *Phys. Rev. B* **76** 224409
[10] Kaneyoshi T 2012 *Phys. Lett. A* **376** 2352
[11] Canko O, Erdinça A, Taşkin F and Atiş M 2011 *Phys. Lett. A* **375** 3547
[12] Jiang W, Guan H Y, Wang Z and Guo A B 2012 *Physica B* **407** 378
[13] Iglesias O and Labarta A 2001 *Phys. Rev. B* **63** 184416
[14] Iglesias O, Batlle X and Labarta A 2005 *Phys. Rev. B* **72** 212401
[15] Vasilakaki M and Trohidou K N 2009 *Phys. Rev. B* **79** 144402
[16] Zaim A and Kerouad M 2010 *Physica A* **389** 3435
[17] Yüksel Y, Aydiner E and Polat H 2011 *J. Magn. Magn. Mater.* **323** 3168
[18] Wesselinowa J M 2010 *J. Magn. Magn. Mater.* **322** 234
[19] Wesselinowa J M and Apostolova I 2008 *J. Appl. Phys.* **104** 084108
[20] Rego L G C and Figueiredo W 2001 *Phys. Rev. B* **64** 144424
[21] Du H F and Du A 2006 *J. Appl. Phys.* **99** 104306
[22] Iglesias O and Labarta A 2006 *Physica B* **372** 24
[23] Keskin M, Şarli N and Deviren B 2011 *Solid State Commun.* **151** 1025
[24] Fonseca F C, Goya G F, Jardim R F, Muccillo R, Carreño N L V, Longo E and Leite E R 2002 *Phys. Rev. B* **66** 104406
[25] Gilles C, Bonville P, Rakoto H, Broto J M, Wong K K W and Mann S 2002 *J. Magn. Magn. Mater.* **241** 430
[26] Crespo P, Litrán R, Rojas T C, Multigner M, Fuente J M, Sánchez-López J C, García M A, Hernando A, Penadés S and Fernández A 2002 *Phys. Rev. Lett.* **93** 087204
[27] Zaim A, Kerouad M and El Amraoui Y 2009 *J. Magn. Magn. Mater.* **321** 1077
[28] Kaneyoshi T 2011 *Phys. Stat. Sol(b)* **248** 250

[29] Kaneyoshi T 2011 *J. Magn. Magn. Mater.* **323** 1145
[30] Usov N A and Gudoshnikov S A 2005 *J. Magn. Magn. Mater.* **290** 727
[31] Du H F and Du A 2007 *Phys. Stat. Sol(b)* **244** 1401
[32] Huang Z, Chen Z, Li S, Feng Q, Zhang F and Du Y 2006 *Eur. Phys. J. B* **51** 65
[33] Deviren B and Keskin M 2012 *Phys. Lett. A* **376** 1011
[34] Deviren B, Kantar E and Keskin M 2012 *J. Magn. Magn. Mater.* **324** 2163
[35] Liu L M, Jiang W, Wang Z, Guan H Y and Guo A B 2012 *J. Magn. Magn. Mater.* **324** 4034
[36] Jiang W, Guan H Y, Wang Z and Guo A B 2012 *Physica B* **407** 378
[37] Zaim A, Kerouad M and Boughrara M 2013 *Solid State Commun.* **158** 76
[38] Jiang W, Liu L M, Li X X, Deng Q, Guan H Y, Zhang F and Guo A B 2012 *Physica B* **407** 3933
[39] Guo A B and Jiang W 2012 *Commun. Theor. Phys.* **58** 772
[40] Huang K 1963 *Statistical Mechanics* (New York: Wiley Press)
[41] Zaim A, Kerouad M and Boughrara M 2013 *J. Magn. Magn. Mater.* **331** 37
[42] Sorop T G, Nielsch K, Göring P, Kröll M, Blau W, Wehrspohn R B, Gösele U and de Jongh L J 2004 *J. Magn. Magn. Mater.* **272** 1656
[43] Cao Z, Ding A, Zhang Y, Qiu P and Zheng W 2004 *Solid State Commun.* **131** 57
[44] Chern G, Horng L, Shieh W K and Wu T C 2001 *Phys. Rev. B* **63** 094421
[45] Zaim A, Kerouad M, Boughrara M, Ainane A and de Miguel J J 2012 *J. Supercond. Nov. Magn.* **25** 2407
[46] Bukharov A A, Ovchinnikov A S, Baranov N V and Inoue K 2010 *J Phys.: Condens. Matter* **22** 436003
[47] Jiang W, Lo V C, Bai B D and Yang J 2010 *Physica A* **389** 2227
[48] Lupu N, Lostun L and Chiriac H 2010 *J. Appl. Phys.* **107** 09E315